Response to Comments from Reviewer 1

We would like to thank the editor and referee for their comments and suggestions on the manuscript. We would also like to answer the questions raised by the report from the reviewer as following.

[Q1] While the paper addresses an important and underexplored topic, it lacks the systematic analysis required for publication in a top-tier journal. A more comprehensive study could include investigations of various defect configurations and models of disorder. (Quoted from the report of Reviewer 1)

[A1] **Following the referee's suggestion, in addition to the isotropic impurity, we also investigate the effect of triangular and square defect configurations on the vortex cluster phase in the revised manuscript.** We start from the Ginzburg-Landau (GL) free energy functional of two-gap superconductors

$$F=\sum_i\left[-\alpha_i\left|\Psi_i\right|^2+\frac{\beta_i}{2}\left|\Psi_i\right|^4+\frac{1}{2m_i}\left|\left(-\mathrm{i}\hbar\nabla-\frac{2e}{c}\mathbf{A}\right)\Psi_i\right|^2\right]+\frac{\mathbf{B}^2}{8\pi}\ . \tag{1}$$

Here Ψ_i $(i=1,2)$ represents the superconducting order parameter and m_i is the effective mass for each band. The coefficient α_i is a function of temperature, while β_i is independent of temperature. In the presence of the T_c disorder (T_c : the critical temperature), the parameters α_1 and α_2 can be approximately expressed as $\alpha_i=\alpha_{i0}g(\mathbf{r})$. Here we introduce a function $g(\mathbf{r})$ between -1 and $+1$ to model the defect potential which will deplete the superconducting state at specific positions. $\mathbf{B}=\nabla\times\mathbf{A}$ is the magnetic field and $\mathbf{A}$ the vector potential.

Then, the time-dependent Ginzburg-Landau (TDGL) equations of the multi-component superconducting system can be derived from

$$-\Gamma_i\frac{\partial\Psi_i}{\partial t}=\frac{\delta F}{\delta\Psi_i^*}\qquad\text{and}\qquad-\sigma_n\frac{\partial\mathbf{A}}{\partial t}=\frac{\delta F}{\delta\mathbf{A}} \tag{2}$$

where Γ_i is the relaxation time of order parameters and σ_n represents the electrical conductivity of the normal sample in the two-band case. Therefore, minimization of the free energy F with respect to Ψ_i and $\mathbf{A}$ leads to the following dimensionless TDGL equations in the zero electrostatic potential gauge

$$-\Gamma_1\frac{\partial\Psi_1}{\partial t}=-\left[g(\mathbf{r})-\left|\Psi_1\right|^2\right]\Psi_1+\left(-\mathrm{i}\nabla-\mathbf{A}\right)^2\Psi_1, \tag{3}$$

$$-\Gamma_2\frac{\partial\Psi_2}{\partial t}=-\left[\frac{\alpha_{20}}{\alpha_{10}}g(\mathbf{r})-\frac{\beta_2}{\beta_1}\left|\Psi_2\right|^2\right]\Psi_2+\frac{m_1}{m_2}\left(-\mathrm{i}\nabla-\mathbf{A}\right)^2\Psi_2 \tag{4}$$

and

$$-\frac{\partial\mathbf{A}}{\partial t}=\kappa_1^2\nabla\times\nabla\times\mathbf{A}-\mathbf{J}_s \tag{5}$$

with the supercurrent

$$\mathbf{J}_s=\left[\frac{\mathrm{i}}{2}(\Psi_1\nabla\Psi_1^*-\Psi_1^*\nabla\Psi_1)-\left|\Psi_1\right|^2\mathbf{A}\right]+\frac{m_1}{m_2}\left[\frac{\mathrm{i}}{2}(\Psi_2\nabla\Psi_2^*-\Psi_2^*\nabla\Psi_2)-\left|\Psi_2\right|^2\mathbf{A}\right]. \tag{6}$$

Here in the clean limit with the impurity function $g=1$, we introduce the coherence length $\xi_i^2=\hbar^2/\left(2m_i\alpha_{i0}\right)$, the London penetration depth $\lambda^{-2}=\lambda_1^{-2}+\lambda_2^{-2}$ with $\lambda_i^{-2}=4\pi e^2\Psi_{i0}^2/(m_ic^2)$ and $\Psi_{i0}=\sqrt{\alpha_{i0}/\beta_i}$, and the GL parameter $\kappa_1=\lambda_1/\xi_1$. We then take the coordinate $\mathbf{r}$ in units of ξ_1, the time t in units of $t_0=m_1\sigma_n/\left(4e^2\Psi_{10}^2\right)$, Γ_i in units of $\alpha_{10}t_0$ and the order parameter Ψ_i in units of Ψ_{10}. We also set the magnetic field $\mathbf{B}$ in units of $H_0=\Phi_0/\left(2\pi\xi_1^2\right)$ with the flux quantum $\Phi_0=\pi\hbar c/e$ and the vector potential $\mathbf{A}$ in units of $A_0=H_0\xi_1$.

Based on the two-band TDGL equations (3)-(5), we can now perform numerical calculations on the effect of impurity on collective vortex patterns with the finite element method. In the procedure of simulations, we set the GL parameters $\Gamma_1=\Gamma_2=5$, $m_1=2m_2$, $\alpha_{10}=\alpha_{20}$ and $\beta_1=\beta_2$. The triangular or square impurity is with a side length of ξ_1 and placed at the center of the $15\xi_1\times15\xi_1$ mesoscopic superconducting system. We take the impurity function as

$$g\left(\mathbf{r}\right)=\begin{cases}-0.5, & \text{inside the impurity}\\ 1, & \text{otherwise}\end{cases}. \tag{7}$$

For the external magnetic field $H_e=0.8H_0$, we plot the magnetic field intensity B_z and the order parameter of the first condensate $\left|\Psi_1\right|$ at $t=10^4t_0$ for triangular and square defect configurations in Fig. 1 and Fig. 2 respectively. With the GL parameter κ_1 taken as 0.70, 1.30 and 2.10 sequentially, we can clearly observe the transitions of this system from the perfect diamagnetism state to the vortex cluster phase, and ultimately to the vortex

lattice phase. For the triangular (or square) impurity case, the peculiar vortex cluster is generated around the pinning site within the range $1.15 < \kappa_1 < 1.52$ (or $1.03 < \kappa_1 < 1.62$). It can be seen from Fig. 1(b,e) that the introduction of triangular defect breaks the C_4 rotational symmetry of the mesoscopic system and will form a distorted cluster in this circumstance. In contrast, the presence of square impurity ensures that the vortex pattern will still preserve the C_4 rotational symmetry, as shown in Figs. 2(b,e) and 2(c,f). Also see Subsection 4.3 "Vortex cluster phase in the presence of an anisotropic impurity" from page 11 to page 12 in the revised version of manuscript.

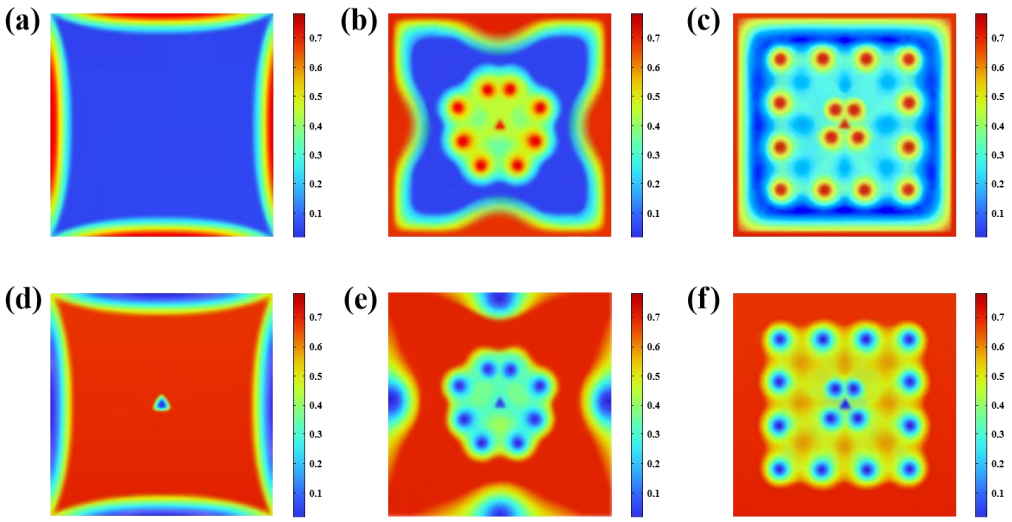

Figure 1: Transitions of the magnetic field intensity B_z (a-c) and the order parameter of the first condensate $|\Psi_1|$ (d-f) in the presence of a triangular defect in the $15\xi_1 \times 15\xi_1$ type-1.5 superconductor. The snapshots show the Meissner phase (a,d), vortex cluster phase (b,e) and vortex lattice phase (c,f) at the GL parameter $\kappa_1 = 0.70$, 1.30 and 2.10 respectively. The magnetization only has the component perpendicular to the superconducting plane.

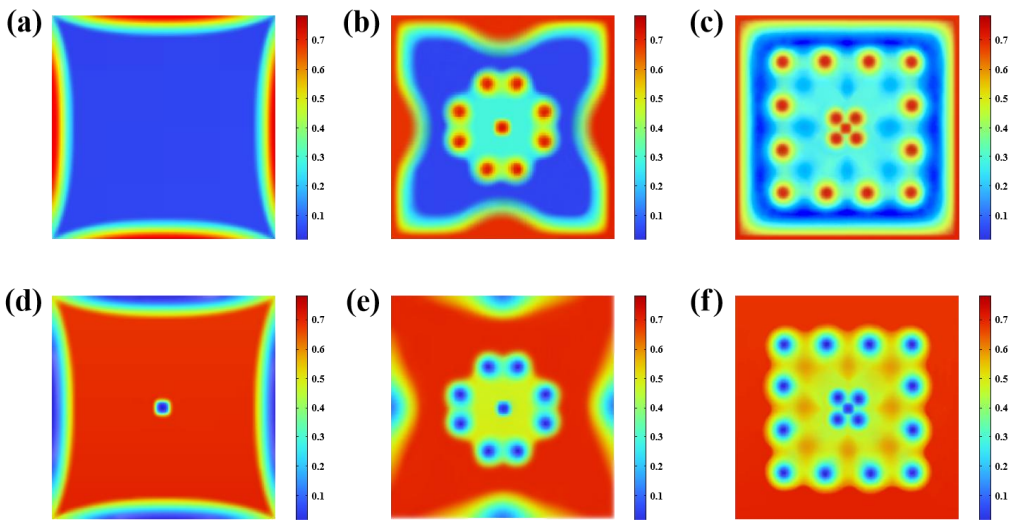

Figure 2: Transitions of the magnetic field intensity B_z (a-c) and the order parameter of the first condensate $|\Psi_1|$ (d-f) at the presence of a square defect in the $15\xi_1 \times 15\xi_1$ type-1.5 superconductor. The snapshots show the Meissner phase (a,d), vortex cluster phase (b,e) and vortex lattice phase (c,f) at the GL parameter $\kappa_1 = 0.70$, 1.30 and 2.10 respectively. The magnetization only has the component perpendicular to the superconducting plane.

Secondly, in order to demonstrate the robustness of vortex cluster phase induced by the localized impurity in the type-1.5 superconductor, we compare the numerical results obtained from two types of disorder models, i.e., the T_c disorder model and the l disorder model (l : the mean free path) in the revised manuscript. Starting from the seminal works of Thuneberg [E.V. Thuneberg, Elementary pinning potential in type II superconductors near H_{c2}, J. Low Temp. Phys. 57, 415 (1984); E.V. Thuneberg, Elementary pinning potentials in superconductors with anisotropic Fermi surface, Cryogenics 29, 236 (1989)], two main disorder models have been proposed to describe the effect of nonmagnetic impurities on the superconducting system in the framework of the GL theory [G. Blatter, M.V. Feigel'man, V.B. Geshkenbein, A.I. Larkin and V.M. Vinokur, Vortices in high-temperature superconductors, Rev. Mod. Phys. 66, 1125 (1994); M. Friesen and P. Muzikar, Microscopic theory of vortex pinning: impurity terms in the Ginzburg-Landau free energy, Phys. Rev. B 53, R11953 (1996)]. The first one is the T_c disorder model as discussed above, which is characterized by altering the GL free energy coefficient $\alpha_i \to \alpha_{i0} g(\mathbf{r})$ in Eq. (1) [S.Z. Lin, S. Maiti and A. Chubukov, Distinguishing between

s+id and *s+is* pairing symmetries in multiband superconductors through spontaneous magnetization pattern induced by a defect, Phys. Rev. B 94, 064519 (2016)]. The other one is the l disorder model, achieved by modifying the effective mass $1/m_i \to (1/m_i)h(\mathbf{r})$ in Eq. (1), where $h(\mathbf{r}) = l/l_m < 1$ represents the ratio of the mean free path inside and outside the well-defined pinning area [J.Y. Ge, J. Gutierrez, V.N. Gladilin, J.T. Devreese and V.V. Moshchalkov, Bound vortex dipoles generated at pinning centres by Meissner current, Nat. Commun. 6, 6573 (2015)].

Now we can systematically discuss the effects of these two disorder models on magnetic vortex patterns in the $15\xi_1 \times 15\xi_1$ type-1.5 superconductor. For the T_c disorder model, we choose the impurity function g to take the phenomenological form

$$g(\mathbf{r}) = \begin{cases} -0.5, & \text{if } |\mathbf{r} - \mathbf{r}_0| < 0.5\xi_1 \\ 1, & \text{otherwise} \end{cases}. \tag{8}$$

It is easy to see that this circular defect is centered at $\mathbf{r}_0 = (x_0, y_0)$. For simplicity, we insert this pinning site at the center of the superconducting square. For $H_e = 0.8H_0$, we plot the magnetic field intensity B_z and the order parameter of the first condensate $|\Psi_1|$ at $t = 10^4 t_0$ in Fig. 3. With the GL parameter κ_1 taken as 0.70, 1.30 and 2.10 sequentially, we can clearly observe the transitions of this type-1.5 system from the perfect diamagnetism state to the vortex cluster phase, and ultimately to the Abrikosov lattice phase. Our numerical simulations also show that the cluster phase presents the vortex pattern with octagonal symmetry and appears in the region of $1.08 < \kappa_1 < 1.58$. Moreover, it can be seen from Fig. 3(c,f) that the isotropic defect induces the localized distortion of the Abrikosov flux lattice, but will still preserve the C_4 rotational symmetry of the superconducting system.

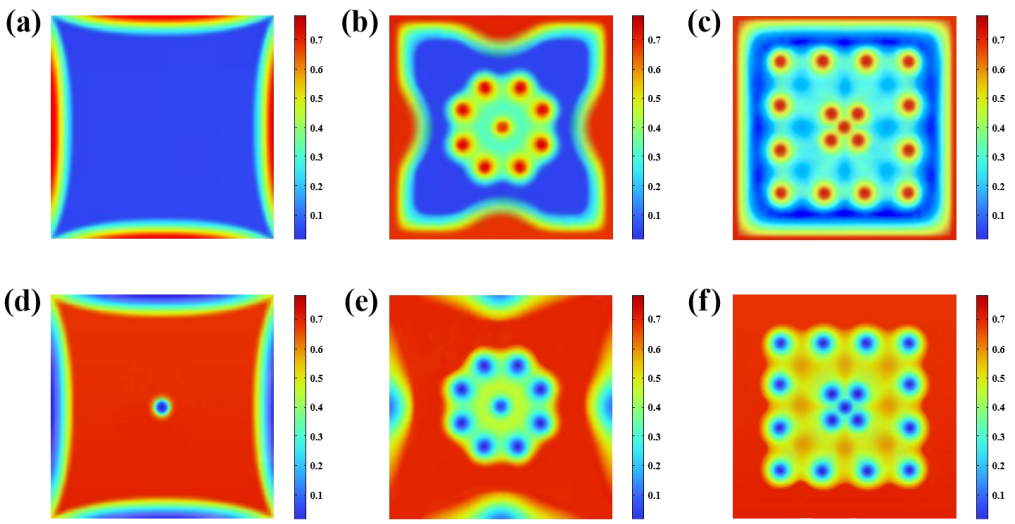

Figure 3: Transitions of the magnetic field intensity B_z (a-c) and the order parameter of the first condensate $|\Psi_1|$ (d-f) for the T_c disorder model at the presence of an isotropic defect in the $15\xi_1 \times 15\xi_1$ type-1.5 superconductor. The snapshots show the Meissner phase (a,d), vortex cluster phase (b,e) and vortex lattice phase (c,f) at the GL parameter $\kappa_1 = 0.70$, 1.30 and 2.10 respectively. The magnetization only has the component perpendicular to the superconducting plane.

For the l disorder model, we set the impurity function h as

$$h(\mathbf{r}) = \begin{cases} 0.2, & \text{if } |\mathbf{r}-\mathbf{r}_0| < 0.5\xi_1 \\ 1, & \text{otherwise} \end{cases}. \tag{9}$$

Then, we also insert this pinning site at the center of the $15\xi_1 \times 15\xi_1$ mesoscopic sample. With $H_e = 0.8H_0$, the magnetic field intensity B_z and the order parameter of the first condensate $|\Psi_1|$ at $t = 10^4 t_0$ are plotted in Fig. 4. For the GL parameter $\kappa_1 = 1.30$ and 2.10, we can observe a vortex cluster pattern with octagonal symmetry in Fig. 4(b,e) and the locally distorted flux lattice with C_4 rotational symmetry in Fig. 4(c,f) respectively. For this particular disorder model, the vortex cluster phase is generated around the pinning site within the range $1.06 < \kappa_1 < 1.59$. **Based on the numerical results mentioned above, we can conclude that within the framework of the GL theory, the T_c and l disorder models are qualitatively equivalent in describing the local effect of the impurity on collective vortex behaviors for the type-1.5 superconductor.** Also see lines 5-12 of the second paragraph on page 3, the first and second paragraphs as well as Figure 4 on page 9,

and Figure 5 on page 10 in the revised version of manuscript.

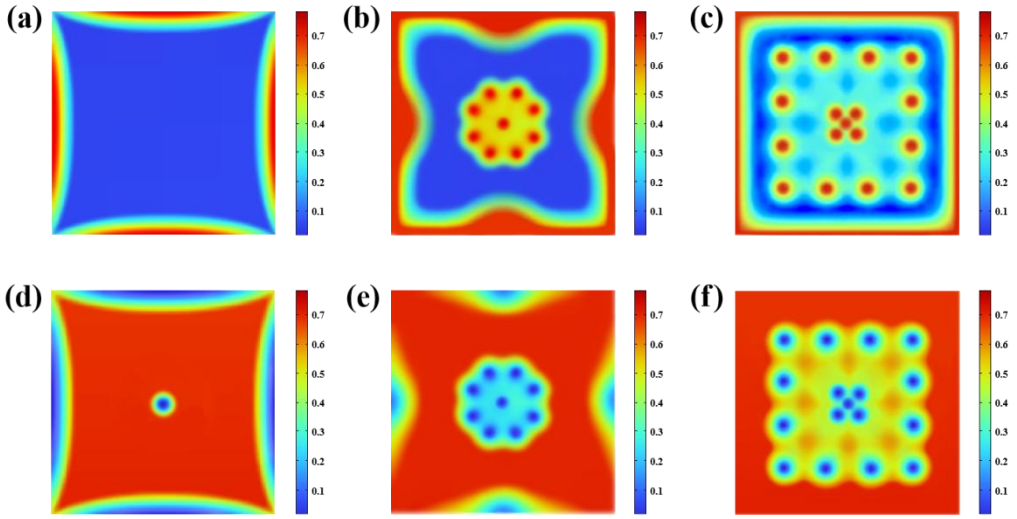

Figure 4: Transitions of the magnetic field intensity B_z (a-c) and the order parameter of the first condensate $|\Psi_1|$ (d-f) for the l disorder model at the presence of an isotropic defect in the $15\xi_1 \times 15\xi_1$ type-1.5 superconductor. The snapshots show the Meissner phase (a,d), vortex cluster phase (b,e) and vortex lattice phase (c,f) at the GL parameter $\kappa_1 = 0.70$, 1.30 and 2.10 respectively. The magnetization only has the component perpendicular to the superconducting plane.

[Q2] For instance, vortex clustering can arise not only from attractive intervortex interactions but also as a consequence of pinning or disorder. The authors could explore whether there exists a critical disorder strength, or density of pinning centers, where the role of attractive interactions becomes particularly significant. (Quoted from the report of Reviewer 1)

[A2] **Firstly, in the absence of impurity, we present the L-κ_1 phase diagram of the two-band superconductor with L the sample size in Fig. 5.** We perform the corresponding numerical calculations based on the two-band TDGL theory (3)-(5). In the procedure of simulations, we set the GL parameters $\Gamma_1 = \Gamma_2 = 5$, $m_1 = 2m_2$, $\alpha_{10} = \alpha_{20}$ and $\beta_1 = \beta_2$. It can be seen from Fig. 5 that with the decrease of L, the vortex cluster phase produced by the long-range attractive interaction between vortices gradually vanishes. Meanwhile, we also notice the critical sample size L_c for the disappearance of this cluster state is $32\xi_1$. **Thus, the superconducting system will stay in the type-1.5 regime above**

L_c and the type-II regime below L_c in the absence of impurity.

As we know, the type-1.5 superconductor originates from a peculiar vortex interaction that exhibits short-range repulsion and long-range attraction characteristics. The obtained critical L_c is consistent with the characteristic length scale (about $30\xi_1$) of the crossover from the attractive to repulsive intervortex interaction [J. Carlström, E. Babaev and M. Speight, Type-1.5 superconductivity in multiband systems, Phys. Rev. B 83, 174509 (2011)]. For the sample size $L > L_c$, the long-range attractive potential between vortices will dominate at the external magnetic field $H_e = 0.8H_0$ and the system is allowed to spontaneously form the stable vortex cluster. However for $L < L_c$, the repulsive intervortex interaction will prevail in the mesoscopic superconductor and the vortex cluster phase can only be induced by other effects such as impurities.

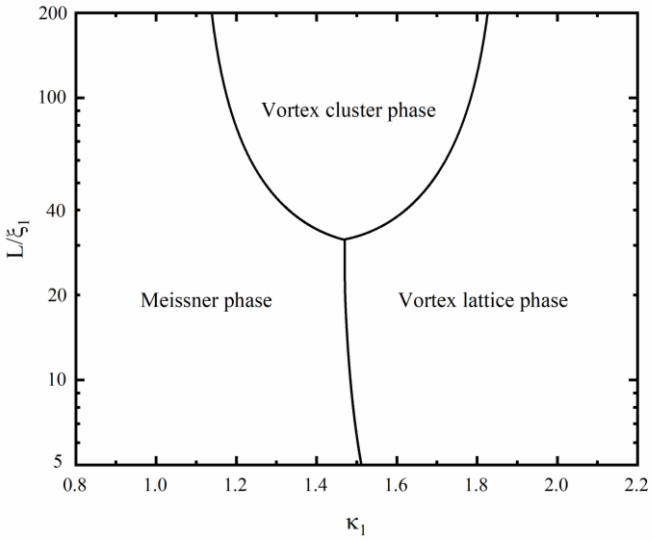

Figure 5: The $L-\kappa_1$ phase diagram of the two-band superconductor in the absence of impurity. We set the external magnetic field $H_e = 0.8H_0$ in the numerical simulations, and plot the sample size L on a logarithmic scale.

Secondly, in the presence of impurity, we will show the g-κ_1 phase diagram of the two-band superconductor with the sample size below L_c in Fig. 6. Here we introduce an isotropic impurity with the radius $0.5\xi_1$ into the $15\xi_1 \times 15\xi_1$ mesoscopic superconducting sample. With the T_c disorder model, the defect function $g(\mathbf{r})$ will be characterized by the disorder strength g inside the impurity. We still insert this circular

impurity at the center of the superconducting square. It can be seen from Fig. 6 that with the increase of the absolute value of g, the vortex cluster phase induced by the attractive interaction from the impurity will gradually appear in the system. Meanwhile, we also see that there indeed exists a critical impurity strength $g_c \approx -0.22$ for the generation of the vortex cluster state in this $15\xi_1 \times 15\xi_1$ sample. **Thus, this mesoscopic superconductor will stay in the type-1.5 regime for $|g| > |g_c|$ and the type-II regime for $|g| < |g_c|$ in the presence of an isotropic impurity.** Also see the third paragraph on page 6, the first paragraph and Figure 1 on page 7, the first paragraph and Figure 3 on page 8 in the revised version of manuscript.

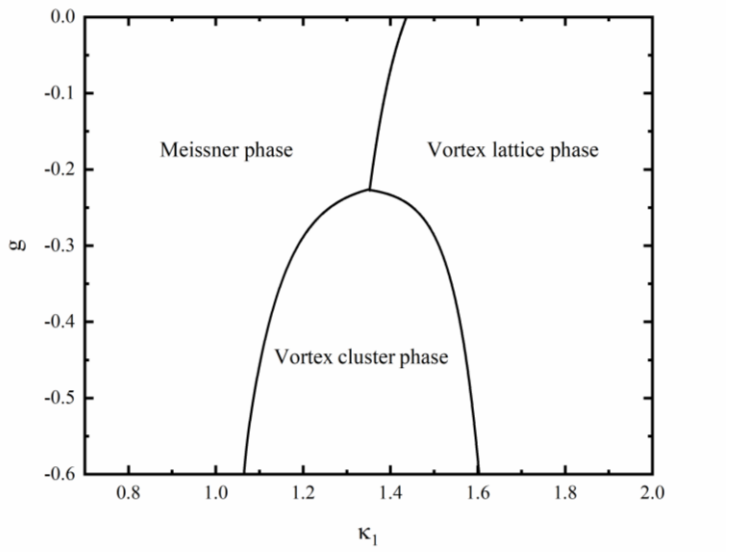

Figure 6: The $g - \kappa_1$ phase diagram of the $15\xi_1 \times 15\xi_1$ two-band superconductor in the presence of an isotropic impurity. We set the external magnetic field $H_e = 0.8H_0$ in the numerical simulations.

[Q3] Additionally, a comparative analysis of type-II and type-1.5 vortex systems under different disorder models would add valuable context and broader relevance to the study. The inclusion of both correlated and uncorrelated disorder is also interesting. With the current material, the paper is suitable for publication in some journal, but not yet at the level of a leading one. A more systematic approach, as outlined above, would strengthen its impact and contribution to the field. (Quoted from the report of Reviewer 1)

[A3] **Firstly, under the T_c and l disorder models, we will give a comparative**

analysis of both the type-1.5 and type-II behaviors for the $15\xi_1 \times 15\xi_1$ mesoscopic superconductor. We perform the corresponding numerical calculations based on the two-band TDGL theory (3)-(5). In the procedure of simulations, we also set the GL parameters $\Gamma_1 = \Gamma_2 = 5$, $m_1 = 2m_2$, $\alpha_{10} = \alpha_{20}$ and $\beta_1 = \beta_2$. For the T_c disorder model, we take the disorder strength $g = -0.5$ ($|g| > |g_c|$) inside an isotropic impurity with the radius $0.5\xi_1$ **in the type-1.5 regime**. Meanwhile, for the l disorder model, we set the corresponding impurity function $h = 0.2$ ($h < h_c$) inside the impurity **in the type-1.5 regime**. Here h_c stands for the critical disorder strength for the formation of the vortex cluster state in the l disorder model, which is estimated as 0.6 from our numerical simulations. Our computational results under these two disorder models are shown in Fig. 3 on page 6 and Fig. 4 on page 7 respectively. With the gradual increase of κ_1, we can clearly observe the transitions from the perfect diamagnetism state to the vortex cluster phase, and ultimately to the Abrikosov lattice phase in Fig. 3 and Fig. 4. Therefore, we conclude that these two disorder models are qualitatively consistent in describing the type-1.5 superconducting behaviors.

At the same time, **in the type-II regime**, we take the defect strength $g = -0.1$ for the T_c disorder model and $h = 0.8$ for the l disorder model inside each isotropic impurity. We still insert this pinning site at the center of the $15\xi_1 \times 15\xi_1$ superconducting square. For $H_e = 0.8H_0$, we plot the magnetic field intensity B_z and the order parameter of the first condensate $|\Psi_1|$ at $t = 10^4 t_0$ in Fig. 7 and Fig. 8. With the GL parameter κ_1 taken as 0.70 and 2.10 sequentially, we can observe the direct transition of the system from the perfect diamagnetic state to the Abrikosov lattice phase in Fig. 7 and Fig. 8. Based on the numerical calculations mentioned above, we can see that both the T_c and l disorder models give the similar results for the type-II system. Also see the first paragraph on page 10, Figure 6 and Figure 7 on page 11 in the revised version of manuscript.

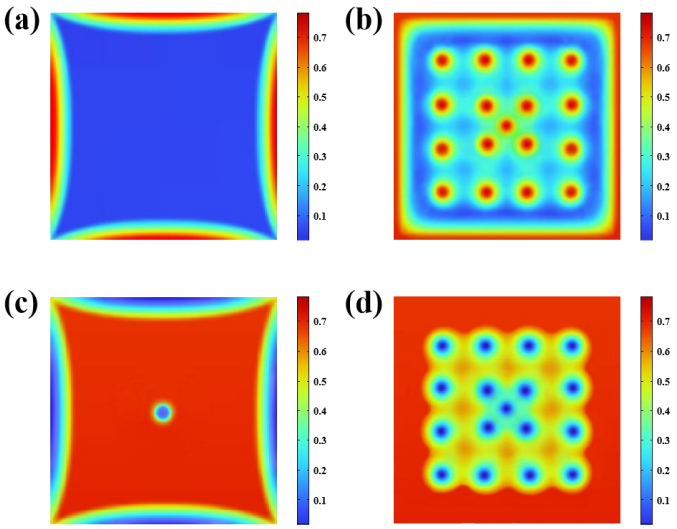

Figure 7: Transition of the magnetic field intensity B_z (a,b) and the order parameter of the first condensate $|\Psi_1|$ (c,d) for the T_c disorder model at the presence of an isotropic defect in the $15\xi_1 \times 15\xi_1$ type-II superconductor. The snapshots show the Meissner phase (a,c) and vortex lattice phase (b,d) at the GL parameter $\kappa_1 = 0.70$ and 2.10 respectively. The magnetization only has the component perpendicular to the superconducting plane.

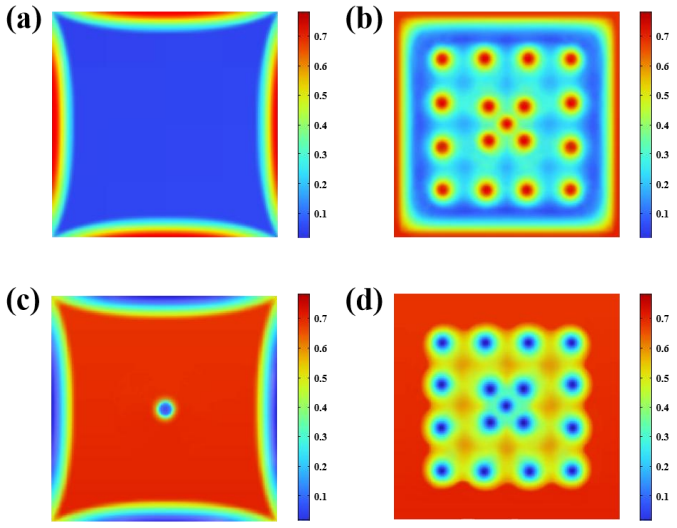

Figure 8: Transition of the magnetic field intensity B_z (a,b) and the order parameter of the first condensate $|\Psi_1|$ (c,d) for the l disorder model at the presence of an isotropic defect in the $15\xi_1 \times 15\xi_1$ type-II superconductor. The snapshots show the Meissner phase (a,c) and vortex lattice phase (b,d) at the GL parameter $\kappa_1 = 0.70$ and 2.10 respectively. The magnetization only has the component perpendicular to the superconducting plane.

Secondly, we set the disorder strength $|g|>|g_c|$ at the impurity sites in the T_c disorder model, and then investigate the effect of multiple uncorrelated and correlated defects on vortex cluster patterns in the $15\xi_1\times15\xi_1$ mesoscopic superconductor. In the **uncorrelated** case, we choose the impurity function $g(\mathbf{r})$ to take the phenomenological form

$$g(\mathbf{r})=\prod_{n=1}^{N}g_n(\mathbf{r}) \qquad \text{with} \qquad g_n(\mathbf{r})=\begin{cases}-0.5, & \text{if } |\mathbf{r}-\mathbf{r}_{0n}|<0.5\xi_1\\ 1, & \text{otherwise}\end{cases}. \tag{10}$$

It is easy to see from Eq. (10) that the isotropic impurity is centered at $\mathbf{r}_{0n}=(x_{0n},y_{0n})$ with $n=1,2,3\cdots N$. For simplicity, we take the impurity number $N=2$ and select the pinning centers at $(\pm3\xi_1,0)$ in $15\xi_1\times15\xi_1$ superconducting sample, which ensures the uncorrelation between these two defects. With $H_e=0.8H_0$, we plot the magnetic field intensity B_z and the order parameter of the first condensate $|\Psi_1|$ at $t=10^4t_0$ in Fig. 9. Different from the single impurity case, multiple vortex clusters are generated around the pinning sites within $0.87<\kappa_1<1.77$. With the GL parameter $\kappa_1=1.30$, we can see from Fig. 9(b,e) that each vortex cluster exhibits the identical pattern with hexagonal symmetry. Meanwhile for $\kappa_1=2.10$, as shown in Fig. 9(c,f), we can clearly observe the localized distortions around the pinning positions in the flux lattice due to the attraction of vortices by impurities.

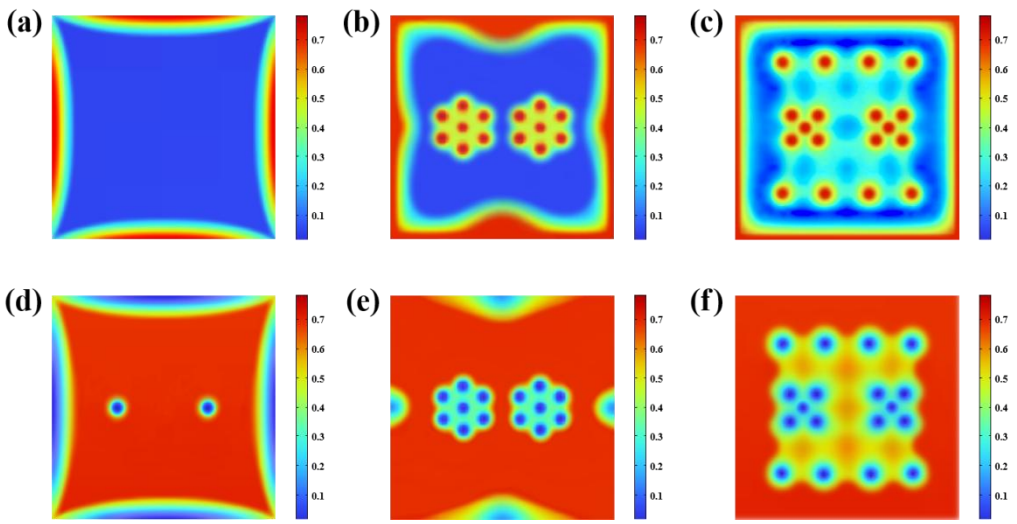

Figure 9: Transitions of the magnetic field intensity B_z (a-c) and the order parameter of the first condensate $|\Psi_1|$ (d-f) at the presence of two uncorrelated defects in the $15\xi_1 \times 15\xi_1$ type-1.5 superconductor. The snapshots show the Meissner phase (a,d), multiple cluster phase (b,e) and vortex lattice phase (c,f) at the GL parameter $\kappa_1 = 0.70$, 1.30 and 2.10 respectively. The magnetization only has the component perpendicular to the superconducting plane.

In order to take into account **the spatial correlation** between these impurities, we choose the following continuous pinning function [F.M. Izrailev, A.A. Krokhin and N.M. Makarov, Anomalous localization in low-dimensional systems with correlated disorder, Phys. Rep. 512, 125 (2012); M.P. Sørensen, N.F. Pedersen and M. Ögren, The dynamics of magnetic vortices in type II superconductors with pinning sites studied by the time dependent Ginzburg-Landau model, Physica C 533, 40 (2017)]

$$g(\mathbf{r}) = \prod_{n=1}^{N} g_n(\mathbf{r}) \qquad \text{with} \qquad g_n(\mathbf{r}) = \tanh\left(\frac{|\mathbf{r} - \mathbf{r}_{0n}| - R}{R_0}\right). \tag{11}$$

We take $R = 0.5\xi_1$, $R_0 = 1.5\xi_1$ in Eq. (11) and then perform numerical simulations in the $15\xi_1 \times 15\xi_1$ mesoscopic superconductor. For comparison with the uncorrelated case, we still choose the defect centers at $(\pm 3\xi_1, 0)$. For $H_e = 0.8H_0$, we plot the magnetic field intensity B_z and the order parameter of the first condensate $|\Psi_1|$ at $t = 10^4 t_0$ in Fig. 10. Note that with this new impurity function, we can obtain the stable vortex cluster phase within $0.92 < \kappa_1 < 1.71$. For $\kappa_1 = 1.30$, it is shown in Fig. 10(b,e) that two vortex clusters

induced by uncorrelated disorders in Fig. 9(b,e) are fused into a single larger cluster here. Meanwhile with $\kappa_1 = 2.10$, we can find a vortex lattice pattern with local distortions around the impurities in Fig. 10(c,f). Also see Subsection 4.4 "Uncorrelated and correlated disorder systems" from page 13 to page 14 in the revised version of manuscript.

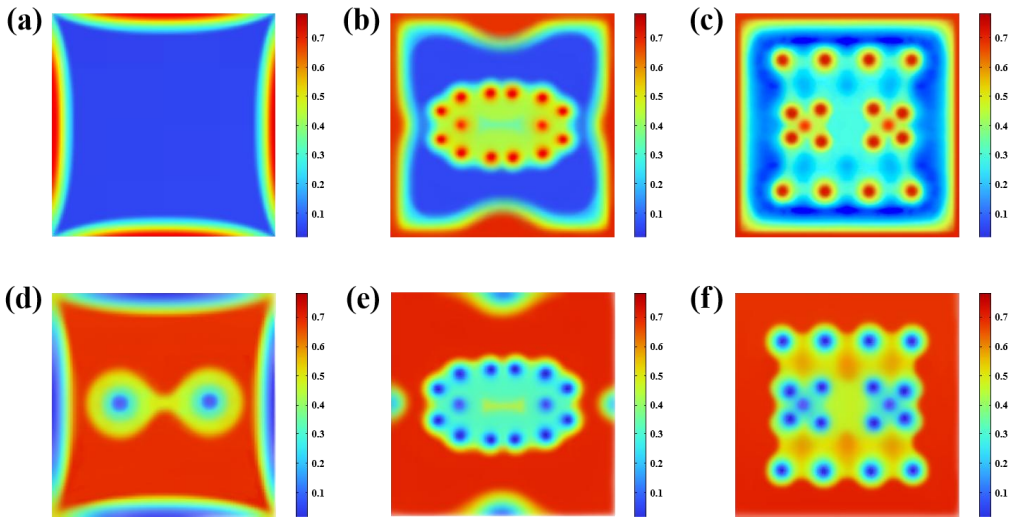

Figure 10: Transitions of the magnetic field intensity B_z (a-c) and the order parameter of the first condensate $|\Psi_1|$ (d-f) at the presence of two correlated defects in the $15\xi_1 \times 15\xi_1$ type-1.5 superconductor. The snapshots show the Meissner phase (a,d), vortex cluster phase (b,e) and vortex lattice phase (c,f) at the GL parameter $\kappa_1 = 0.70$, 1.30 and 2.10 respectively. The magnetization only has the component perpendicular to the superconducting plane.

[Q4] The authors state: "As we know, each condensate in two-band superconductors is predicted to support vortex excitation with fractional quantum flux [4,5]." However, this statement is problematic. Reference [4] does not actually consider fractional vortices; instead, it deals with an infinitely thin loop. For such a configuration, the enclosed flux is effectively zero. The misinterpretation in [4] arises from the assumption that the phase winding can differ from an integer multiple of 2π, which is incorrect. (Quoted from the report of Reviewer 1)

[A4] We are very grateful to the referee for this invaluable explanation. In Reference [4] [Y. Tanaka, Soliton in two-band superconductor, Phys. Rev. Lett. 88, 017002 (2002)], as the referee pointed out, the vortex excitation with fractional quantum flux actually arises from

the incorrect assumption that the phase winding can differ from an integer multiple of 2π around a loop configuration. Taking this point into account, we will only cite Reference [5] [E. Babaev, Vortices with fractional flux in two-gap superconductors and in extended Faddeev model, Phys. Rev. Lett. 89, 067001 (2002)] in the statement mentioned above. Also see lines 1-2 of the second paragraph on page 2 in the revised version of manuscript.

[Q5] Additionally, the authors should update their discussion to acknowledge recent experimental advances. A Science paper published in 2023 and two preprints from 2024 report experimental observations of fractional vortices. (Quoted from the report of Reviewer 1)

[A5] We thank the referee for this helpful suggestion. Based on the scanning superconducting quantum interference device (SQUID), Iguchi *et al*. first detected the temperature-dependent fractional vortices in the hole-overdoped superconductor $Ba_{0.23}K_{0.77}Fe_2As_2$ [Y. Iguchi, R.A. Shi, K. Kihou, C.H. Lee, M. Barkman, A.L. Benfenati, V. Grinenko, E. Babaev and K.A. Moler, Superconducting vortices carrying a temperature-dependent fraction of the flux quantum, Science 380, 1244 (2023)]. Later on, Zhou *et al.* enhanced the SQUID sensitivity and further measured the dynamic process in which a single quantum vortex splits into two spatially separated fractional vortices in the same iron-based superconducting material [Q.Z. Zhou, B.R. Chen, B.K. Xiang, I. Timoshuk, J. Garaud, Y. Li, K.Y. Liang, Q.S. He, Z.J. Li, P.H. Zhang, K.Z. Yao, H.X. Yao, E. Babaev, V. Grinenko and Y.H. Wang, Observation of single-quantum vortex splitting in the $Ba_xK_{1-x}Fe_2As_2$ superconductor, arXiv: 2408. 05902 (2024)]. Furthermore, Zheng *et al*. directly captured the fractional quantum vortex cores on the potassium terminated surface of multiband superconductor KFe_2As_2 by the scanning tunneling microscopy [Y. Zheng, Q.X. Hu, H.J. Ji, I. Timoshuk, H.X. Xu, Y.W. Li, Y. Gao, X. Yu, R. Wu, X.Y. Lu, V. Grinenko, E. Babaev, N.F.Q. Yuan, B.Q. Lv, C.M. Yim and H. Ding, Direct observation of quantum vortex fractionalization in multiband superconductors, arXiv: 2407. 18610 (2024)]. We have cited these recent experimental advances in the revised manuscript, also see lines 5-7 of the second paragraph on page 2 in the revised version of manuscript.